Key Points:
- Satellite-derived temperature trends over 1979–2014 agree well with the WACCM chemistry-climate model
- Ensemble model simulations (five members) give quantitative estimates of internal variability for temperature trends
- Robust temperature response to stratospheric ozone depletion and partial recovery is found in observations and WACCM simulation

Correspondence to:
W. J. Randel,
randel@ucar.edu

Troposphere-Stratosphere Temperature Trends Derived From Satellite Data Compared With Ensemble Simulations From WACCM

William J. Randel[1] , Lorenzo Polvani[2] , Fei Wu[1], Douglas E. Kinnison[1] , Cheng-Zhi Zou[3], and Carl Mears[4]

[1]National Center for Atmospheric Research, Boulder, CO, USA, [2]Department of Applied Physics and Applied Mathematics, Columbia University, New York, NY, USA, [3]Center for Satellite Applications and Research, NOAA/NESDIS, College Park, MD, USA, [4]Remote Sensing Systems, Santa Rosa, CA, USA

Abstract Decadal-scale trends in tropospheric and stratospheric temperatures derived from satellite measurements over 1979–2014 are compared with ensemble simulations from the Whole Atmosphere Community Climate Model (WACCM). The model is forced with observed sea surface temperatures, changes in greenhouse gases, and ozone-depleting substances, plus solar and volcanic effects, and results from five WACCM realizations (with slightly different initial conditions) are analyzed. We focus on the vertical structure of tropospheric warming and stratospheric cooling increasing with height, the latitudinal and seasonal dependence of trends, and on the temporal evolution of stratospheric temperatures in response to stratospheric ozone depletion and partial recovery. The model captures the observed trend structure in most respects, and the ensemble of simulations provides quantitative estimates of the impact of internal variability on trend estimates. In regions of low variability (e.g., over low latitudes) the ensemble mean trends agree with the observations, while in regions of high variability (e.g., the polar stratosphere) the observations mostly fall within the range of realizations. Temperature response to evolving stratospheric ozone is evaluated by computing separate trends over 1979–1997 (ozone depletion) and 1998–2014 (partial recovery). Robust changes in temperature trends between these periods occur in the global upper stratosphere and in the Antarctic spring lower stratosphere, with consistent behavior between model and observations. Observed lower stratospheric temperatures in the Antarctic show statistically significant warming after 1998, reflecting recently reported healing of the ozone hole.

Plain Language Summary This work compares temperature trends during 1979–2014 measured by satellites with results from a state-of-the-art chemistry-climate model, incorporating observed forcings including observed sea surface temperatures and changes in greenhouse gases and ozone-depleting substances, plus solar cycle and volcanic effects. We analyze an ensemble of five different model simulations (with slightly different initial conditions) to evaluate effects of internal climate variability on temperature trends. Temperature trends show good quantitative agreement between model and observations, including troposphere warming and stratosphere cooling increasing with altitude. This agreement demonstrates that the satellite-observed temperature changes are a result of known forcings, both natural and anthropogenic. Stratospheric temperatures reflect the influence of stratospheric ozone depletion and partial recovery, with stronger cooling during the first half of the record. Satellite measurements identify a warming of the Antarctic lower stratosphere since 1998, as a response to the recently reported "healing" of the Antarctic ozone hole.

1. Introduction

Global atmospheric temperatures have been continuously measured by satellites since late 1978, and satellite data provide ongoing measurements to monitor and evaluate observed variability and trends. The radiative effects of increasing greenhouse gases (GHG) and changes in stratospheric ozone as a response to human emissions of ozone-depleting substances (ODS) have led to a net warming of the troposphere and cooling of the stratosphere (Hartmann et al., 2013). The detailed vertical structure of tropospheric warming and stratospheric cooling, together with the spatial and temporal variations of associated temperature changes, serves as fingerprints of the relevant forcing processes (e.g., Santer et al., 2013).

Comparisons of observations to comprehensive model simulations are an important aspect of evaluating and understanding model behavior and providing confidence for future predictions. The goal of this paper is to
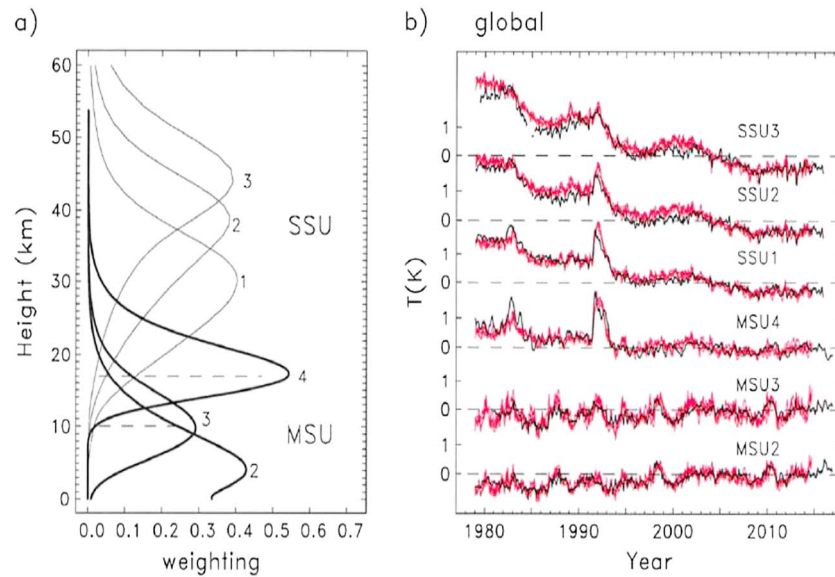
Figure 1. (a) Weighting functions for the MSU and SSU satellite measurements. The dashed lines near 17 km and 10 km indicate the approximate altitudes of the tropical and extratropical tropopause. (b) Time series of global average deseasonalized temperature anomalies for each of the MSU and SSU channels. Black lines shows observations (from STAR MSU and SSU + MLS data), and red lines show overlaid results from the five separate WACCM realizations.

present some basic comparisons of the historical satellite data record with simulations from a state-of-the-art chemistry-climate model, incorporating observed forcings including observed sea surface temperatures (SSTs), GHG, and ODS changes, solar cycle and other aspects as detailed below. We focus on quantifying several key features or "fingerprints" of temperature trends, including the vertical structure of tropospheric warming and stratospheric cooling, latitudinal and seasonal variations in trends, and the evolution of stratospheric temperatures in response to changing ozone. Our work builds on similar evaluations of model simulations from the Coupled Model Intercomparison Project (CMIP5) (Taylor et al., 2012) and the Stratospheric Processes and their Role in Climate (SPARC) Chemistry-Climate Model Validation activity (CCMval) (Stratospheric Processes and their Role in Climate, 2010), such as shown in Forster et al. (2011), Gillett et al. (2011), Mitchell (2016), Seidel et al. (2011), Thompson et al. (2012), and Zhao et al. (2016). The focus of these latter papers is primarily on the stratospheric temperature behavior, as a complement to detailed studies of tropospheric evolution (such as analyzed in Santer et al., 2017, and references therein). Novel aspects of our study include evaluations spanning both the troposphere and stratosphere, based on recently updated and improved satellite data sets, and focus on the variability within an ensemble of simulations from a single chemistry-climate model, constrained with observed forcings but free to evolve from slightly different initial conditions. Using an ensemble of model realizations provides a measure of internal climate variability on estimates of trends from the satellite observational record beginning in 1979 and complements comparisons of runs from numerous different climate models (e.g., Forster et al., 2011; Thompson et al., 2012).

2. Data and Analyses

2.1. Satellite Observations

Our analyses compare model simulations with long-term temperature measurements from six separate satellite channels spanning the troposphere and stratosphere, with weighting functions shown in Figure 1a. Lower altitude measurements are from the Microwave Sounding Unit (MSU) combined with Advanced Microwave Sounding Unit (AMSU) data (hereafter simply MSU). MSU data are from three channels with weighting functions approximately 10 km thick, peaking at altitudes near 4, 10, and 18 km (MSU2, MSU3, and MSU4, respectively; Figure 1a). Note that MSU4 spans the upper troposphere and lower stratosphere in the tropics (~30°N-S), but mainly the lower stratosphere over higher latitudes, while MSU3 covers the troposphere in the tropics but combines the upper troposphere and lower stratosphere in extratropics;
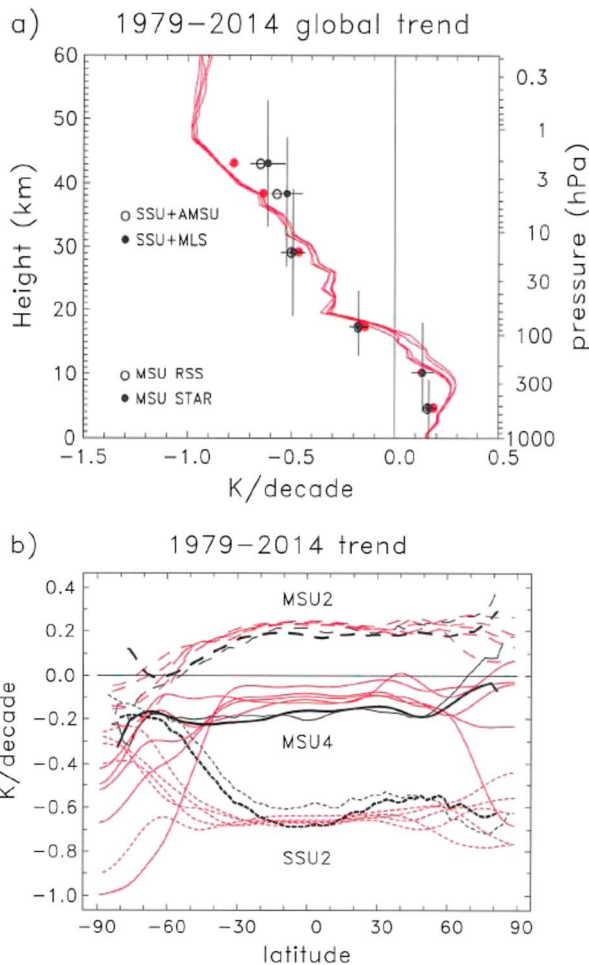
Figure 2. (a) Vertical profile of annual mean global average temperature trends over 1979–2014 derived from satellite measurements and the WACCM realizations. Dots show results from MSU2, MSU3, and MSU4 and SSU1, SSU2, and SSU3 (bottom to top), with separate data sets as noted. Red dots indicate WACCM ensemble profile trends sampled with the respective satellite weighting functions. Vertical bars denote the vertical weighting of the satellite measurements, and horizontal bars show 2 sigma statistical uncertainties. Results are not included for RSS MSU3 because these data are unavailable before 1987. (b) Latitudinal profiles of temperature trends over 1979–2014 for MSU2, MSU4, and SSU2, from observations (black lines) and the WACCM realizations (red lines). Thick (thin) black lines denote results from RSS (STAR) MSU data, and SSU + AMSU (SSU + MLS) data, respectively.

note the tropical and extratropical tropopause heights included in Figure 1a. We utilize two separate MSU observational data sets, obtained from Remote Sensing Systems (RSS) (http://www.remss.com), described in Mears and Wentz (2009), and Mears and Wentz (2016), and NOAA Center for Satellite Applications and Research (STAR) (http://www.star.noaa.gov), described in Zou et al. (2006) and Zou and Wang (2011). Data from MSU2 and MSU3 are from RSS v4.0 retrievals (Mears & Wentz, 2016), while MSU4 uses RSS v3.3. We use retrieval version 4.0 for the STAR MSU data (Zou & Wang, 2011). We analyze monthly mean data spanning the period January 1979 to December 2014, because the Whole Atmosphere Community Climate Model (WACCM) simulations end in 2014. MSU3 data are only available after 1981 from STAR and after 1987 from RSS. Both data sets are provided with a 2.5° latitude resolution; STAR data cover 88.75 N-S, while RSS data cover 82.5 N-S. In general, the MSU data from STAR and RSS give very similar results, aside from some differences in polar regions, as shown below.

Middle and upper stratosphere temperatures are from the stratospheric sounding unit (SSU) which ends in 2005; merged data over 1979–2005 are described in Zou et al. (2014). The SSU measurements are from three channels with broad vertical weighting functions ~20 km thick, peaking near 30, 37, and 43 km (Figure 1a). These time series are updated to 2014 by combining with vertically weighted temperatures from Aura Microwave Limb Sounder (MLS) measurements, as described in Randel et al. (2016); hereafter these data are termed SSU + MLS. An independent set of updated SSU data has been produced by Zou and Qian (2016), based on utilizing AMSU to extend the SSU measurements after 2005 (termed SSU + AMSU). We include results based on both SSU + MLS and SSU + AMSU data sets for comparison below. McLandress et al. (2015) have also produced a merged data set from SSU + AMSU measurements (their data end in 2012), but we focus here on the Zou and Qian (2016) results.

2.2. WACCM Simulations

The Community Earth System Model version 1 (CESM1), Whole Atmosphere Community Climate Model (WACCM), is a coupled chemistry climate model that extends from the Earth's surface to the lower thermosphere (Garcia et al., 2007; Kinnison et al., 2007; Marsh et al., 2013). WACCM is superset of the Community Atmosphere Model, version 4 (CAM4), and includes all of the physical parameterizations of CAM4 (Neale et al., 2013) and a finite volume dynamical core (Lin, 2004) for the tracer advection. The horizontal resolution is 1.9° latitude × 2.5° longitude, and there are 66 vertical levels over 0–120 km. Simulations used in the work are based on the International Global Atmospheric Chemistry/Stratosphere-troposphere Processes And their role in Climate (SPARC) Chemistry Climate Model Initiative (CCMI) (Morgenstern et al., 2017). Improvements in CESM1 (WACCM) for CCMI includes a modification to the orographic gravity wave forcing that reduced the cold bias in Antarctic polar temperatures (Calvo et al., 2017; Garcia et al., 2017) and updates to the stratospheric heterogeneous chemistry which improved the representation of polar ozone depletion (Solomon et al., 2015; Wegner et al., 2013). In this work, the REF-C1 scenario (Morgenstern et al., 2017) was followed and five ensemble members were completed spanning the period between years 1955 and 2014. This scenario includes forcing of greenhouse gases (CH_4, N_2O, and CO_2), organic halogens, volcanic surface area density and heating, and 11 year solar cycle variability. The sea surface temperatures are based on observations (updated from Hurrell et al., 2008), and the quasi-biennial oscillation (QBO) is nudged to observed monthly mean tropical winds over 86–4 hPa, as described in Matthes et al. (2010).

Table 1

MSU2 and MSU3 Temperature Trends (K/Decade) Over 1979–2014 and 2 Sigma Uncertainties (in Brackets)

Data set	Global average	20°N-S
RSS MSU2	0.16 (0.04)	0.18 (0.05)
STAR MSU3	0.13 (0.05)	0.16 (0.07)
STAR MSU2	0.16 (0.04)	0.21 (0.06)
WACCM MSU3	0.13 (0.02)	0.22 (0.02)
WACCM MSU2	0.19 (0.02)	0.23 (0.03)

Note. Results are shown for the global average and over the deep tropics (20°N-S). WACCM trends and uncertainties are for the ensemble mean results. MSU3 trends are not shown for RSS data because the time series do not begin until 1987.

2.3. Analyses

Our analyses focus on comparisons of WACCM to the broad layer satellite temperature measurements. For direct comparisons we vertically integrate the WACCM temperature profiles using the corresponding satellite weighting functions in Figure 1a. While the actual SSU weighting functions are weakly dependent on latitude (e.g., Zou & Qian, 2016), for simplicity we use constant weighting functions (similarly for MSU). Linear trends are derived from the satellite observations and model results using a standard multivariate linear regression analyses used in stratospheric studies (e.g., Seidel et al., 2016). The statistical model includes terms for linear trends, 11 year solar cycle with a proxy of the solar radio flux at 10.7 cm ($F_{10.7}$), quasi-biennial oscillation (QBO) based on two orthogonal QBO indices following Wallace et al., 1993, and El Nino–Southern Oscillation (ENSO) using the multivariate ENSO index (MEI) (Wolter & Timlin, 2011) obtained from http://www.esrl.noaa.gov/enso/mei. The MEI is an optimized ENSO proxy based on sea level pressure, surface temperatures and winds, and cloudiness; zonal mean temperatures are lagged 1 month with respect to the MEI proxy to give the highest correlations. Linear trends are calculated for the full period 1979–2014 and separately for two subperiods (1979–1997 and 1998–2014), the latter to investigate the influence of stratospheric ozone evolution (ozone depletion followed by partial recovery). Our regression analyses exclude periods strongly influenced by large volcanic eruptions of El Chichón (April 1982) and Mount Pinatubo (June 1991) by simply omitting data for 2 years following each eruption. Statistical trend uncertainties are evaluated using a bootstrap resampling technique (Efron & Tibshirani, 1993). For the ensemble WACCM calculations (based on five realizations), mean trends are the average of the five realizations and uncertainties are estimated as the root-mean-square of uncertainties from
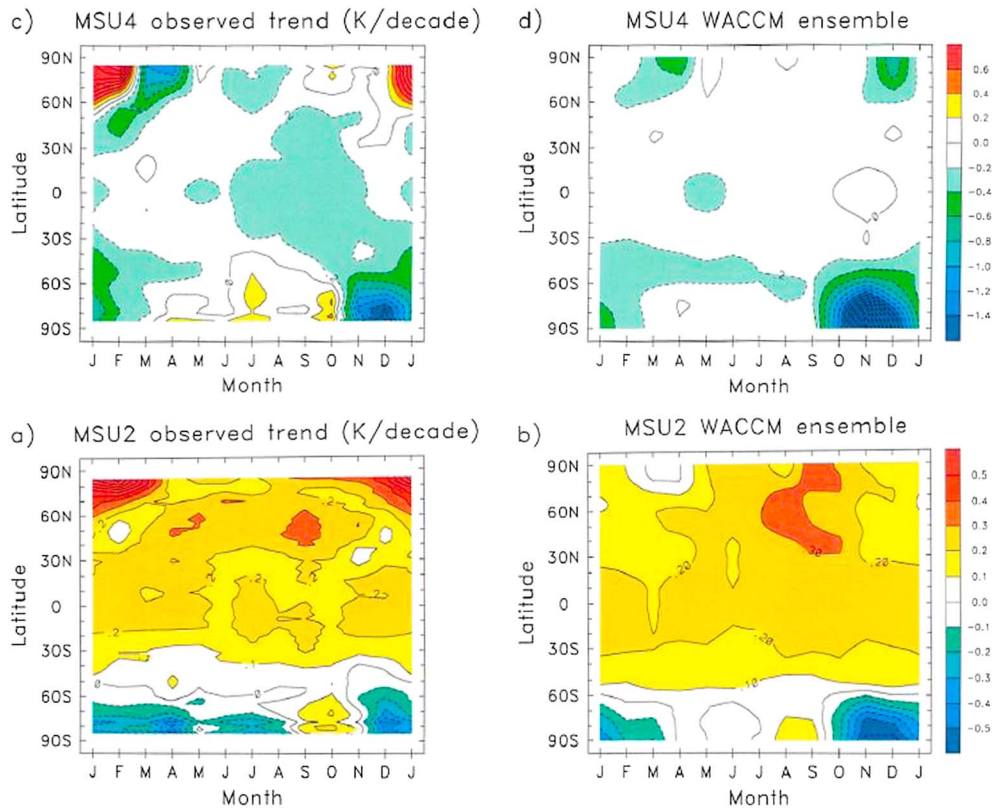

Figure 3. Latitude versus month temperature trends (K/decade) over 1979–2014 for (c and d) MSU4 and (a and b) MSU2, from observations (Figures 3a and 3c) and ensemble WACCM results (Figures 3b and 3d). Observational results are based on STAR MSU data.
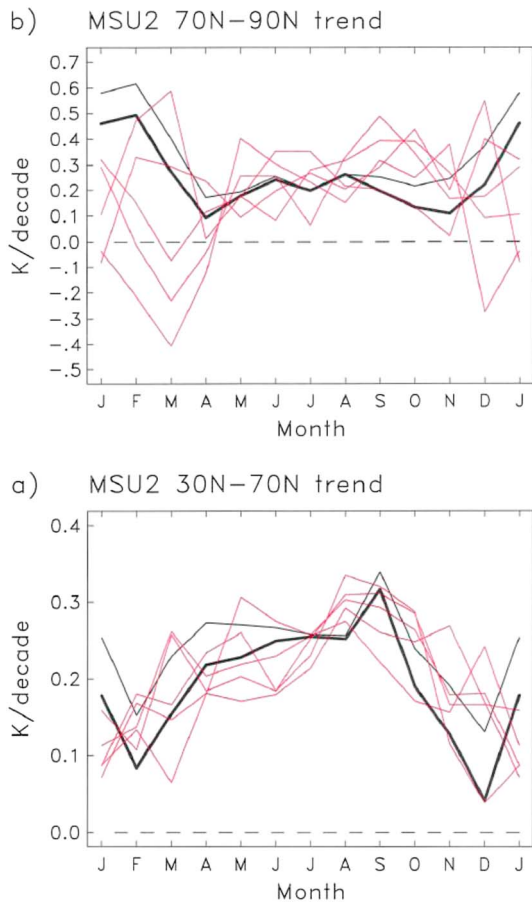
Figure 4. Monthly variation of MSU2 temperature trends for latitude bands (a) 30–70°N and (b) 70–90°N. Black lines show observations (thick: RSS and thin: STAR) and red lines show the WACCM realizations.

the five realizations, and hence, ensemble uncertainties are smaller by approximately a factor of $(1/\sqrt{5})$ compared to the individual simulations (e.g., Santer et al., 2008).

3. Results

3.1. Trends for 1979–2014

Time series of global averaged deseasonalized temperature anomalies for each satellite channel are shown in Figure 1b, comparing observations with WACCM results for each of the realizations. Overall, the global average model time series over 1979–2014 show excellent agreement with observations for each of the satellite channels and relatively small spread among realizations. This means that the observed global changes are a response to natural and anthropogenic forcings, not the result of internal variability. Key features in the global time series include net warming in the troposphere (MSU2 and MSU3) and cooling in the stratosphere that increases with altitude. Time series also highlight episodic volcanic warming in the lower stratosphere (MSU4 and SSU1) and coherent variations in the troposphere (MSU2 and MSU3) tied to ENSO events which are forced by specified SSTs and hence similar among the WACCM realizations. For comparison, similar time series averaged over the deep tropics (20°N-S) are shown in Figure A1a; there is relatively small spread of variability in the WACCM results for the troposphere (MSU2 and MSU3), highlighting the importance of the imposed SSTs for tropical tropospheric temperatures.

The vertical profile of global average temperature trends calculated over 1979–2014 is shown in Figure 2a, comparing the WACCM realizations versus broad layer satellite estimates. The satellite-based trends show good agreement between the different data sets, that is, between STAR and RSS for MSU channels and between SSU + MLS and SSU + AMSU for SSU channels. There is reasonable agreement between the observed and modeled temperature trends (tropospheric warming and stratospheric cooling) and small spread among th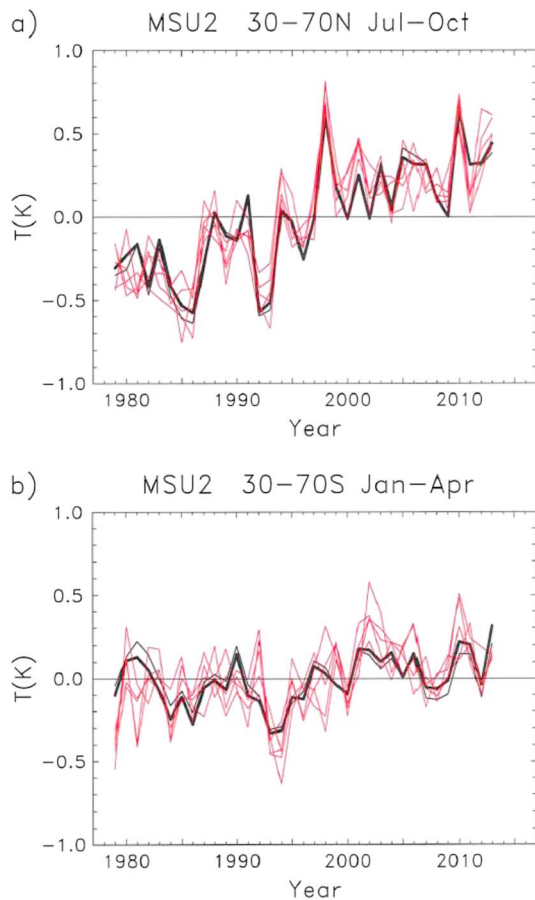e WACCM ensemble members for the global average, aside from the layer over ~10–17 km. The model shows slightly stronger warming in the troposphere than observed in MSU2, and this is discussed further below. The model also exhibits a somewhat stronger increase of cooling with altitude in the upper stratosphere than inferred from the three SSU channels, although the magnitude of cooling is in reasonable agreement.

The latitudinal structure of temperature trends for 1979–2014 is shown in Figure 2b for channels MSU2, MSU4, and SSU2 (troposphere, lower stratosphere, and upper stratosphere, respectively), comparing observations with the WACCM realizations. The observational data sets at each level are in agreement in terms of magnitude and latitudinal structure, with some larger differences over the poles (e.g., MSU2 in the Antarctic). One key result in Figure 2b is that the model realizations show relatively compact spread of temperature trends in low latitudes but large variability in polar latitudes, especially for the stratospheric MSU4 and SSU2 channels. This highlights the large internal dynamic variability of the polar stratosphere during winter-spring in both hemispheres, and therefore, observed trends in the polar regions should not be interpreted as a response to forcings, whether natural or anthropogenic. Over low latitudes individual members of the model and observed trends in Figure 2b show approximate agreement, although with differences in magnitude for each channel.

Tropospheric (MSU2) warming is larger in WACCM than in the observations, which is a difference seen in similar comparisons of numerous climate models (e.g., Santer et al., 2017). MSU2 trends for global means and for the deep tropics (20°N-S) are included in Table 1, comparing RSS, STAR, and WACCM ensemble results; while the satellite-derived trends are systematically smaller than in the model, the statistical uncertainties do overlap at the 2 sigma level, for example, 20°N-S MSU2 trends for WACCM are 0.23 ± 0.03 K/decade, versus 0.18 ± 0.05 for RSS and 0.21 ± 0.06 for STAR data. We note that our derived observational MSU2 trends for

Figure 5. (a) Time series of MSU2 temperature anomalies over the NH extratropics (30–70°N) during boreal summer (July–October). Black lines show observations (thick: RSS and thin: STAR), and red lines show the WACCM realizations. (b) Corresponding MSU2 time series for the SH summer (30–70°S, January–April).

1979–2014 are slightly larger than results in Mears and Wentz (2016) and Santer et al. (2017), although they overlap within uncertainties; these differences occur because of different details in the regression methodologies. This is discussed further in section 4.

Trends derived from MSU3 have not been included in previous troposphere trend comparisons. Our results show that MSU3 trends are positive but somewhat smaller than corresponding MSU2 trends in both the observations and WACCM results, for both global and tropical calculations (see Figures 2a and A1b and Table 1). As with MSU2, the observed and model ensemble trends for MSU3 agree within statistical uncertainties. The smaller MSU3 trends compared to MSU2 in the deep tropics (Figure A1b) are somewhat surprising given the trend increase with height in the troposphere simulated in WACCM (which is expected, e.g., in Santer et al., 2005). However, it turns out that MSU3 trends are strongly influenced by the tail of the weighting function extending into the lower stratosphere (above 20 km; Figure 1a), so that the vertical weighting gives smaller trends than for MSU2.

MSU4 trends show somewhat stronger cooling in observations than in the model in Figure 2b, and similar behavior was noted in the comparisons with numerous models in Thompson et al. (2012). The MSU4 measurements are an average over a region of strong vertical trend gradients (upper tropospheric warming to lower stratospheric cooling, for example, Figures 2a and A1b), and the small observed versus model differences are likely sensitive to the model vertical resolution or other such details. Stronger cooling occurs in the upper stratosphere (SSU2) in both model and observations (~−0.6 K/decade), with relatively small magnitude differences between observations and model; corresponding differences are larger for SSU3 (e.g., Figure 2a). For the most part, observed trends in polar regions in Figure 2b fall within the (large) range of model variability among the realizations, although the observed SSU2 cooling trends are systematically smaller in the Antarctic than the model results. However, given the large variability, five members may not be sufficient to explore the full range of internal variability in the polar stratosphere.

Variations of the latitude-dependent trends as a function of individual month provide a fingerprint of seasonally evolving trends. The seasonal variation of trends over 1979–2014 is shown in Figure 3 for the troposphere (MSU2) and lower stratosphere (MSU4), comparing observations versus the ensemble mean from WACCM. These plots are derived by calculating trends for each individual month and simply contouring the results. Results for tropospheric temperature trends (MSU2; Figures 3a and 3b) show statistically significant warming of magnitude ~0.2 K/decade over latitudes ~30°N-S throughout the year, with maxima extending to northern middle and high latitudes in boreal spring-summer (approximately April–October). The model ensemble shows that the strongest MSU2 warming occurs over ~30–90°N during July–October, and a similar-timed maximum is seen in observations. Strong Arctic wintertime polar warming is found in MSU2 observations (Figure 3a), although this is marginally significant in light of large background variability, and a similar maximum is not evident in the WACCM ensemble (see discussion below). There are weak and insignificant trends for MSU2 over Southern Hemisphere (SH) extratropics in both observations (~35–70°S) and the model (~50–70°S). The ensemble MSU2 WACCM trends in Figure 3b exhibit significant cooling over the Antarctic in October–February, which is vertically coupled to lower stratosphere cooling (tied to the Antarctic ozone hole); note that the MSU2 weighting extends well into the Antarctic lower stratosphere (Figure 1a). This behavior occurs with smaller amplitude in the MSU2 observations (Figure 3a). Overall, the MSU2 observations show consistent behavior to the ensemble WACCM trends in terms of latitude and seasonal structure, with slightly weaker trend magnitudes.

The detailed seasonal variations of MSU2 trends in the Northern Hemisphere (NH) extratropics are interesting in several respects. For the latitude band 30–70°N there is a summertime warming maximum found in both
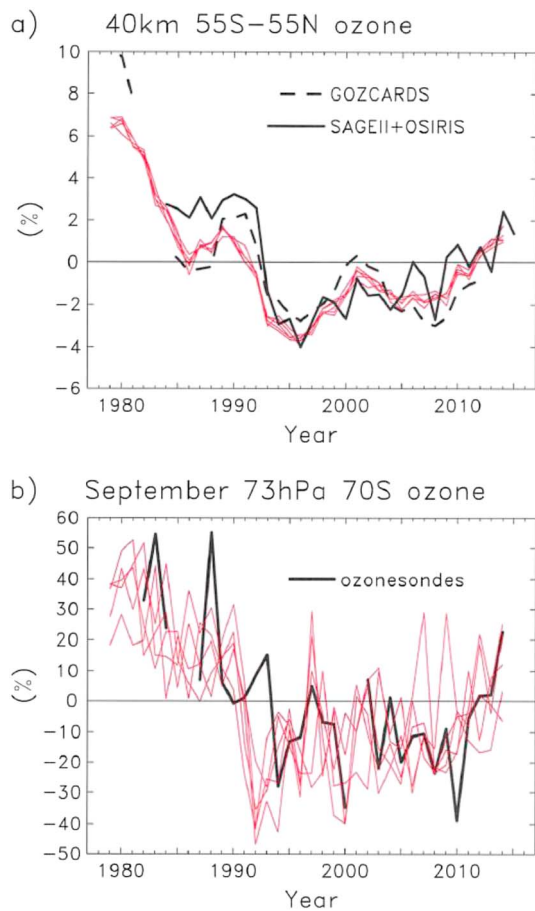
Figure 6. These plots compare ozone variability in WACCM vs. observations. (a) Time series of annual average ozone anomalies at 40 km averaged over 55°N-S, comparing observations from GOZCARDS and merged SAGE II + OSIRIS data sets with the WACCM realizations (red lines). (b) Time series of September ozone anomalies at 73 hPa derived from Syowa (69°S) ozonesondes compared with WACCM zonal means at 70°S.

model and observations (Figure 4a), with relatively small scatter among model realizations suggesting a forced seasonal response. Time series of MSU2 temperature anomalies in this region are shown in Figure 5a (30–70°N, July–October average), showing strong trends with remarkably high interannual correlation between the model and observations. There is little dispersion among the WACCM ensemble members, suggesting that both the interannual variability and the long-term trends in the observations are a response to some external driver, most likely to SSTs which are specified in our model integrations. For comparison, Figure 5b shows the corresponding summer high-latitude time series in the SH (30–70°S, January–April), where there are no significant long-term trends.

MSU2 trends over the Arctic polar cap (70–90°N; Figure 4b) are very different from those over middle latitudes (Figure 4a). Observations show large positive trends in winter (January–March). However, in that season the model trends are widely scattered among the different ensemble members. Note that the MSU2 observations in January–February actually are outside of the ensemble range, although the overall behavior suggests that five realizations may not be enough to capture the range of possible trends. More importantly, the large spread in winter MSU2 trends over the Arctic polar cap is a clear indication that much of the observed trends in that region may be a manifestation of large internal variability and not a forced response to anthropogenic emissions. We also note that the model ensemble trends at individual vertical levels show a strong polar warming maximum during September–January, mainly confined to the near-surface model levels, similar to the "Arctic amplification" behavior discussed in Screen and Simmonds, 2010. However, that autumn-winter polar maximum is absent in the deep MSU2 layer, as seen in the ensemble WACCM trends (Figure 3b); the large positive winter trends in the observations (red corners in Figure 3a) therefore must be interpreted as originating from internal variability.

Latitude versus month patterns of observed 1979–2014 trends for MSU4 (Figure 3c) show weak and marginally significant cooling over the majority of the globe. The observations show a small seasonal cooling maximum in the tropics during approximately July–November, similar to the tropical trends noted in a shorter time series by Free (2011) and Fu et al. (2015), but such a maximum is not see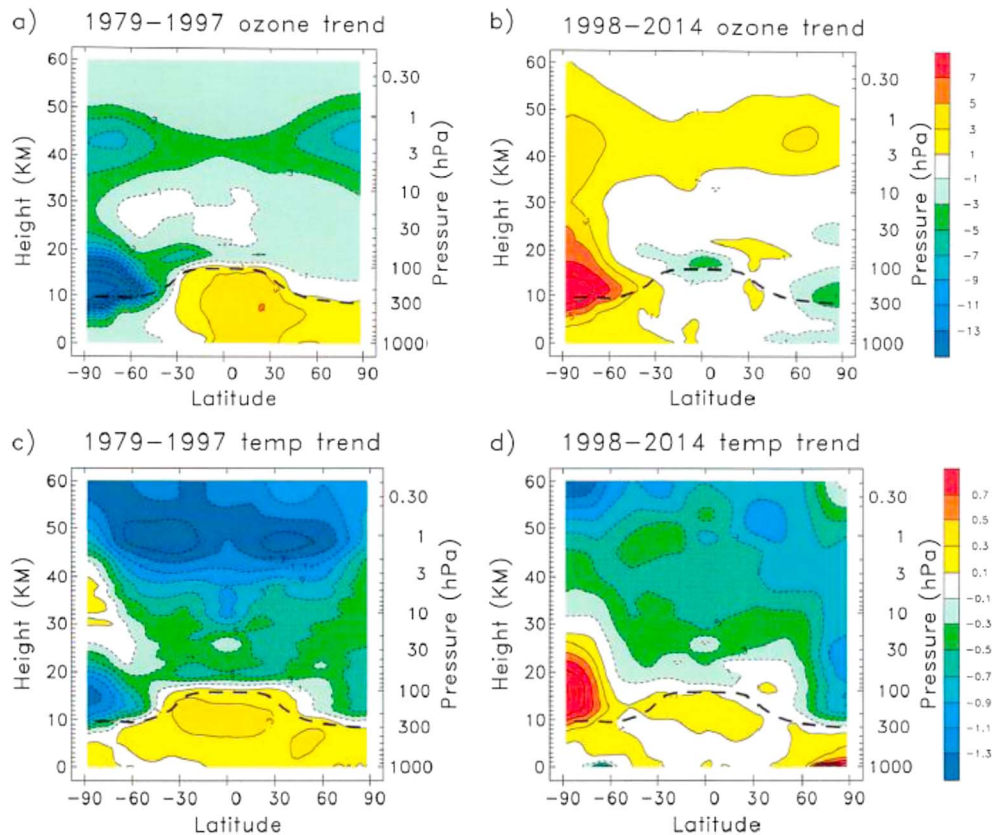n in the WACCM ensemble. Fu et al. (2015) suggest this observed behavior may be related to low-frequency changes in stratospheric Brewer-Dobson circulation, and Polvani and Solomon (2012) suggest that the temperatures may reflect a thermal response to seasonal variations in tropical ozone trends. The strongest and most significant MSU4 cooling trends occur in the Antarctic during spring and summer as a response to the ozone hole. The WACCM ensemble shows polar cooling of ~2–3 K/decade during October–December, with weaker but statistically significant cooling extending into austral summer and covering middle to high latitudes. We note that the Antarctic ozone and temperature changes are better fit using piecewise linear trends, reflecting ozone depletion and partial recovery, as discussed below; the trends over 1979–2014 reflect the dominance of ozone loss compared to recovery through 2014. The observed MSU4 trends (Figure 3c) show similar behavior to the WACCM ensemble over the Antarctic, although with differences in detail, such as no observed cooling in October, a period influenced by large dynamic variability. The MSU4 trends in the Arctic during winter-spring are not statistically significant in either the observations or the WACCM ensemble, and observations show small but significant Arctic summertime cooling.

Upper stratospheric trends (from SSU1, SSU2, and SSU3) show relatively small seasonal variations in low to middle latitudes; results for SSU2 are shown in Figure A2. In polar regions there is large variability and no significant trends during the respective winter-spring seasons in either hemisphere. However, strong and highly significant cooling trends are found in the upper stratosphere during Arctic summer, in a region of low background variability; observations and model simulations agree well in this behavior, with a net cooling of ~3 K

Figure 7. Latitude-height cross sections of ensemble annual average (a and b) ozone and (c and d) temperature trends from WACCM, derived for the periods 1979–1997 (Figures 7a and 7c) and 1998–2014 (Figures 7b and 7d). Ozone trends are in (%/decade) and temperature trends are in K/decade.

over 1979–2014. In the Antarctic summer there are weak and marginally significant cooling trends, with slightly weaker trends in observations compared to the WACCM ensemble.

3.2. Influence of Evolving Stratospheric Ozone

Stratospheric temperatures are expected to respond to stratospheric ozone concentrations, which change in response to halogen loading (e.g., Stolarski et al., 2010). Evidence for evolving stratospheric temperature trends has recently been shown in Aquila et al. (2016), Randel et al. (2016), Polvani et al. (2017), Seidel et al. (2016), and Zou and Qian (2016), based on analysis of MSU and SSU data. Here we evaluate these changes in comparison to WACCM. The calculations are based on piecewise linear trends over 1979–1997 and 1998–2014, and the choice of break point in 1997 is based on similar recent calculations (e.g., Kyrölä et al., 2013). Overall results are not sensitive to this exact breakpoint.

Ozone in the WACCM simulations responds to specified changes in ODS, producing a decrease prior to the late 1990s and an increase thereafter. As a prerequisite to evaluating temperature trends it is important to quantify model ozone changes in comparison to observations. Accordingly, we show in Figure 6a time series of near-global ozone in the model upper stratosphere (~40 km) compared with observations. Figure 6a includes measurements of ozone at 40 km averaged over 55°N-S, derived from merged SAGE II + OSIRIS satellite measurements during 1984–2015 (Bourassa et al., 2017) and also from the GOZCARDS data base (Froidevaux et al., 2015). The model shows good quantitative agreement with observations, highlighting decreases over circa 1979–1997 and (smaller) increases after circa 1998. Figure 6b shows a similar comparison of ozone changes in the Antarctic spring lower stratosphere, comparing September ozonesonde measurements from Syowa (69°S) with WACCM zonal means sampled at 70°S, motivated by similar comparisons in Solomon et al. (2016). The time series show decreases prior to the late 1990s followed by increases after circa 2000, with reasonable agreement between the model and ozonesonde measurements (consistent with
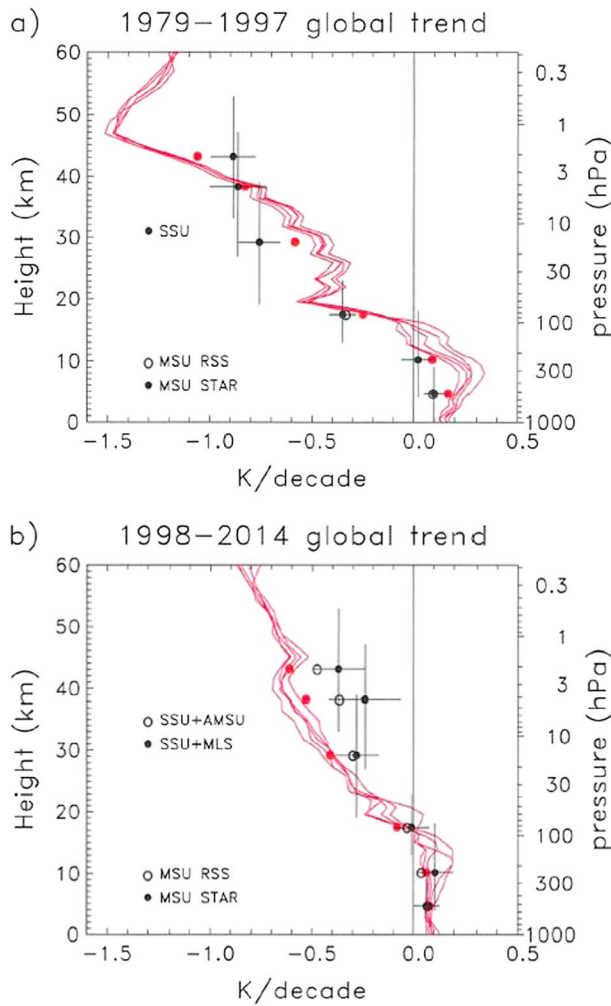
Figure 8. Vertical profiles of global average temperature trends for (a) 1979–1997 and (b) 1998–2014, comparing satellite observations to realizations from WACCM. Details are the same as in Figure 2a.

results in Solomon et al., 2016, 2017). The comparisons in Figures 6a and 6b suggest accurate simulation of ozone changes (decrease and partial recovery) in WACCM for the two subperiods. We focus on quantifying the temperature response to these ozone changes by analysis of trends for these respective subperiods.

The global behavior of annual average ozone and temperature changes in the model for the periods 1979–1997 and 1998–2014 is shown in Figure 7, calculated for the ensemble average. Stratospheric ozone decreases during 1979–1997 (Figure 7a) show maximum percentage decreases in the upper stratosphere (~40 km) and in the Antarctic ozone hole. The upper stratosphere ozone losses occur throughout the year, while the Antarctic lower stratosphere losses are focused in spring. Simulated ozone increases in the troposphere for this period are a response to specified changes in precursor emissions but have small influence on the radiative balance (Stevenson et al., 2013). Stratospheric ozone changes for 1998–2014 (Figure 7b) approximately mirror those for the earlier period with opposite sign (and one third to one half the magnitude), including the global upper stratosphere and the Antarctic ozone hole. Decreasing ozone occurs near the tropical tropopause for both periods, as a response to increasing tropical upwelling (Garcia & Randel, 2008).

Stratospheric temperature changes in the model show the strong influence of ozone evolution. Upper stratosphere cooling is much stronger for the ozone decrease period 1979–1997 (Figure 7c), with maximum trends of ~−1.5 K/decade near 50 km, compared to a maximum of ~−0.6 K/decade for 1998–2014 (Figure 7d). There is also a strong thermal response to ozone changes in the Antarctic, with the (ensemble) model results showing the well-known cooling in the lower stratosphere for 1979–1997 (near −1.2 K/decade for the annual mean), followed by statistically significant warming for the ozone recovery period 1998–2014 (up to 1.0 K/decade near the pole over 10–20 km). It is interesting that the magnitude of model Antarctic temperature trends is similar for the ozone decline and partial recovery periods, although the corresponding ozone changes are much larger for 1979–1997. Relatively weaker cooling for 1979–1997 may reflect compensation from increased downwelling over the polar cap, as suggested in (Calvo et al., 2017, Fu et al., 2010, Ivy et al., 2016, & Lin et al., 2009). We note

that the Arctic lower stratosphere shows marginally significant cooling in the model during this 1998–2014 period, although ozone changes are not significant.

The vertical profiles of global average temperature trends for the ozone depletion and recovery subperiods are shown in Figure 8, comparing the WACCM realizations with satellite measurements; corresponding plots for tropical averages (20°N-S) are shown in Figure A3. Stronger stratospheric cooling occurs for 1979–1997 in both observations and model simulations, with reasonable agreement in magnitude and vertical structure, although the broad layer SSU measurements do not capture the strong vertical gradient suggested by the model. Stratospheric cooling trends are smaller during 1998–2014, and the SSU trends are somewhat weaker in the satellite measurements than in WACCM; there are slightly stronger cooling trends in SSU + AMSU data (closer to WACCM) than in SSU + MLS. It is interesting that the MSU2 and MSU3 tropospheric trends are smaller in observations compared to WACCM for 1979–1997 but agree well for 1998–2014. For the earlier period the model shows tropospheric trends that increase with altitude for all five ensemble members (Figures 8a and A3a), while this is not the case for 1998–2014; both periods show substantial spread among model realizations for tropospheric trends.

The latitudinal profiles of annual average MSU4 and SSU2 trends for the two subperiods are shown in Figure 9. Stronger stratospheric cooling is evident in both channels during the period of ozone loss (1979–1997); the observed and modeled trends agree reasonably well over low latitudes, except for the smaller SSU2 trends
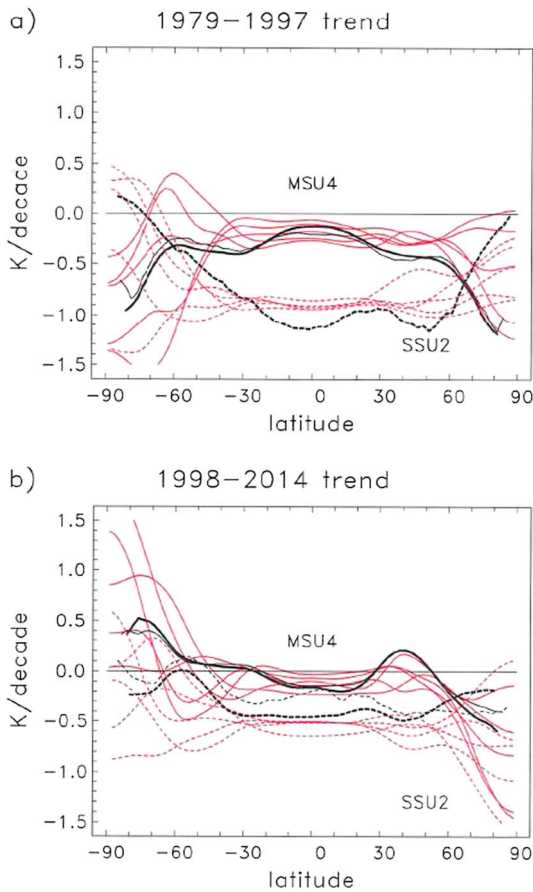
Figure 9. Latitudinal profiles of temperature trends for MSU4 and SSU2, for the periods (a) 1979–1997 and (b) 1998–2014. Details are the same as in Figure 2b.

in SSU + MLS observations for 1998–2014 noted above. In polar regions the model realizations show large variability in trends, which is not surprising for these relatively short time samples, but the observed trends typically fall within the (wide) range of model realizations, indicating the model is able to bracket the observations. For the ozone decline period (Figure 9a), the upper stratosphere (SSU2) shows very small cooling over the poles compared to low latitudes. This behavior is echoed in both observations and model results and is probably a signature of strongest temperature response to ozone depletion over sunlit regions. The observed MSU4 trends show enhanced polar cooling in both hemispheres during 1979–1998; the individual model realizations follow this behavior (with widespread) in the Antarctic, while in the Arctic the model trends span a range from strongly negative to near zero. This indicates that observed Arctic trends over that period cannot be unambiguously attributed to anthropogenic forcings. During 1998–2014 MSU4 trends in the Antarctic are positive for four of the five realizations, consistent with the significant ensemble warming trends in Figure 7d, and observed trends are also positive. The observed annual average MSU4 trends over 70–90°S for 1998–2014 are 0.50 (±0.63) K/decade for RSS data and 0.39 (±0.52) for STAR data (2 sigma uncertainties) and hence not statistically significant.

Monthly variations of the observed and modeled trends over the South Pole (70–90°S) during the ozone decline and recovery periods are shown in Figures 10a and 10b. During 1979–1997 (Figure 10a) cooling occurs during October–December with magnitude ~−2 K/decade in observations and a wide range of ~−2 to −6 K/decade in the WACCM realizations. This is the well-known radiative response to Antarctic ozone depletion (e.g., Gillett & Thompson, 2003; Randel & Wu, 1999; Thompson & Solomon, 2002; Young et al., 2013). While there is substantial variability in cooling magnitude among WACCM realizations, the seasonal pattern within the ensemble is clear. A nearly opposite South Pole temperature trend response is seen for 1998–2014 (Figure 10b), with observed warming of ~2 K/decade during October–November. There is variability among the model realizations, but four of the five show a similarly timed warming temperature response, which occurs due to Antarctic ozone increase in the model, for example, Figure 7b. The observed MSU4 warming trends during the individual months October–December in Figure 10b are marginally significant, and the results are slightly different based on RSS versus NOAA STAR data sets.

Time series of MSU4 temperature anomalies over the South Pole (70–90°S) averaged for October–November are shown in Figure 11, including observational and WACCM results. Dashed lines in Figure 11 indicate the regression fits to the STAR observations and the WACCM ensemble. Trends and statistical uncertainties derived from these data over 1979–1997 and 1998–2014 are included in Table 2, including the ensemble WACCM results. Cooling during the ozone decline period is highly significant in the observations and in approximate agreement with the model. Warming is derived from the observations during 1998–2014, although the magnitude and significance is slightly different depending on the RSS versus STAR MSU4 data sets (2.60 ± 2.38 K/decade in the RSS data and 1.77 ± 1.94 in the STAR data, using 2 sigma uncertainty levels). Nonetheless, while the precise level of warming and degree of significance is different between these data, the overall behavior of evolving Antarctic temperature trends in spring and their congruence with WACCM (e.g., Figure 10) is strong evidence for an observed warming linked to the ozone hole "healing" reported in Solomon et al. (2016).

4. Discussion

This work focuses on detailed comparisons between observed temperature changes derived from historic satellite measurements (1979–2014) with results from an ensemble of five WACCM simulations, using
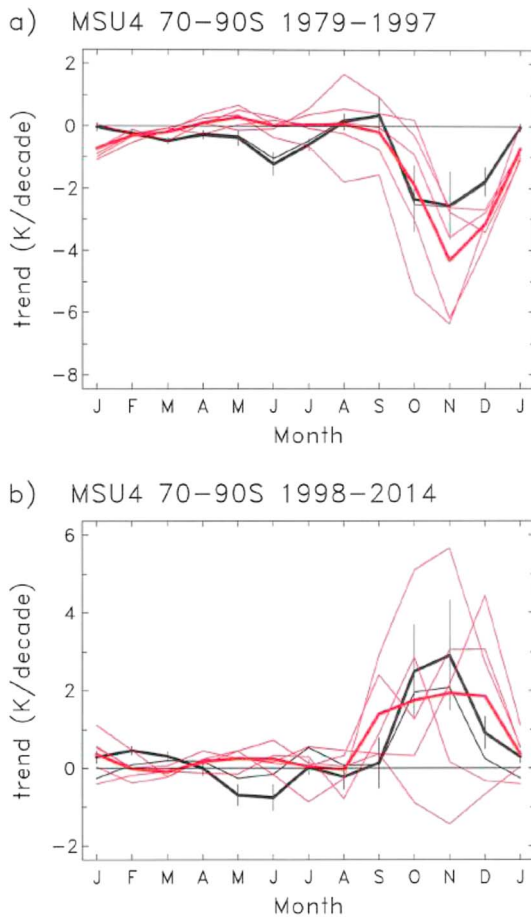
Figure 10. Monthly MSU4 temperature trends near the South Pole (70–90°S) derived for the periods (a) 1979–1997 and (b) 1998–2014, derived from observations and the WACCM realizations. The dark (light) black lines show results from RSS (STAR) MSU4 data, and the error bars show corresponding 1 sigma uncertainties for each month (for clarity, just shown for the RSS results). The dark red line is the WACCM ensemble average.
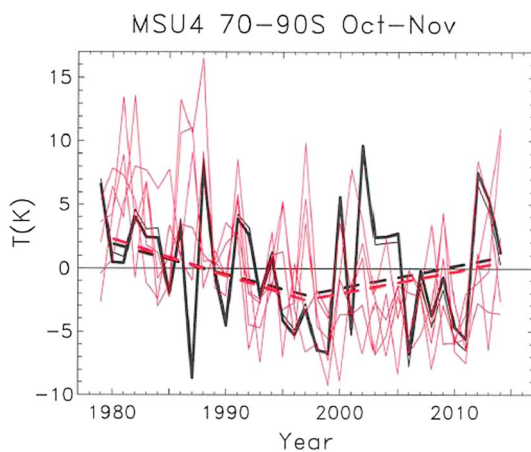

Figure 11. Time series of October–November average MSU4 temperature anomalies near the South Pole (70–90°S), showing results from observations and the WACCM realizations. The dashed lines indicate the trends for the subperiods 1979–1997 and 1998–2014 derived from STAR MSU4 data (black) and WACCM ensemble (red).

observed forcings including observed SSTs, GHG, and ODS changes, solar, and volcanic effects. The analysis of five realizations (with slightly different initial conditions) provides a measure of the influence of internal climate variability on temperature variability and trends and is a complement to comparisons of observations with numerous different climate or chemistry-climate models (e.g., Forster et al., 2011; Santer et al., 2017; Thompson et al., 2012). Our evaluations compare trends from the broad layer MSU and SSU temperature measurements spanning the troposphere and stratosphere with similar layer means derived from the model simulations.

Our comparisons show that the WACCM ensemble results agree with observed temperature trends in almost all respects, within the variability of the realizations. Time series of global average temperature anomalies show excellent agreement between observations and model simulations (Figure 1b). Global average time series highlight tropospheric warming and stratospheric cooling (increasing with altitude), plus variability tied to ENSO, volcanic, and solar effects. Our analyses have focused on temperature trends and not on comparing details of the ENSO, volcanic, or solar effects, although Figure 1b suggests overall reasonable simulations for the global mean behavior of these components. Further comparisons suggest approximate observed versus model agreement in vertical and latitudinal structures for ENSO and solar variations derived via regression. For example, Figure A4 shows the ENSO regression of MSU2 tropospheric temperatures as a function of latitude and month, for STAR observations and WACCM ensemble, showing a tropically centered (~30°N-S) temperature response maximizing in boreal winter in both model and observations. However, the focus of this paper is on temperature trends, and below we discuss some aspects of the key features related to vertical trend structure, latitudinal and seasonal behavior, and evolution related to stratospheric ozone.

4.1. Vertical Structure

The vertical structure of tropospheric warming and stratospheric cooling is the fundamental fingerprint of increasing GHG and stratospheric ozone changes (e.g., Manabe & Wetherald, 1967; Ramaswamy & Schwarzkopf, 2002; Shine et al., 2003). Global average temperature trends during 1979–2014 show excellent agreement between observations and model simulations in this behavior (Figure 2a), with small variability among model realizations. Global average tropospheric warming, as measured by observed 1979–2014 trends in MSU2, is somewhat smaller than corresponding MSU2 trends simulated by WACCM, although the differences are not statistically significant (Table 1). These observed versus model differences for MSU2 are similar to previous results based on comparisons with other climate models (Santer et al., 2017, and references therein), although our comparisons reveal only statistically insignificant trend differences for the forced WACCM simulations. The excellent agreement for WACCM is at least partly attributable to forcing using observed SSTs, which tightly constrain tropospheric temperatures, as compared to free-running atmosphere-ocean climate models (e.g., CMIP5).

We note that our MSU2 global mean and tropical (20°N-S) trends are slightly more positive compared to other calculations based on the same observational data (e.g., Mears & Wentz, 2016; Santer et al., 2017), although results overlap within uncertainty levels. These differences occur because

Table 2

MSU4 Temperature Trends for October–November Averages at the South Pole (70–90°S), Shown in Figure 11

Data set	1979–1997	1998–2014
RSS	−2.30 (2.24)	2.60 (2.38)
STAR	−2.37 (2.18)	1.77 (1.94)
WACCM ensemble	−2.83 (1.00)	1.56 (1.18)

Note. Linear trends (K/decade) and 2 sigma statistical uncertainties (in brackets) are shown for the indicated periods.

the respective regression calculations are somewhat different; following previous stratospheric trend studies, we use a multivariate regression including solar cycle, QBO, and ENSO proxy terms and omit the periods influenced by the volcanic eruptions of El Chichón and Pinatubo. However, our analyses are applied consistently between observations and model results, so that the comparisons shown here are straightforward. We note that Santer et al. (2001) also analyzed the sensitivity of tropospheric regression trend estimates to including ENSO and volcanic effects.

For comparison, we tested our regression calculations using a simple linear fit (trend only) with no additional proxy terms and including the volcanic-perturbed periods, with results shown in Table 3. The simple regression model yields slightly smaller warming trends for MSU2 and MSU3 for both observations and model, and the uncertainties are somewhat larger. However, the conclusions regarding the comparisons of observed versus WACCM trends are the same based on either regression calculation.

We have included comparisons for trends derived from MSU3 (using STAR data, beginning in 1981), which have not been reported previously. Results show statistically significant warming for MSU3 for the global and tropical averages, and agreement within uncertainties with WACCM (Table 1). Warming trends for MSU3 are systematically smaller than for MSU2 in both observations and model, even for the deep tropics where the model shows an increase of trends with height in the troposphere (Figure A1b). In this case the MSU3 trends are smaller than MSU2 because the long tail of the MSU3 weighting function extends into the lower stratosphere (above 20 km) and hence convolves stratospheric cooling with upper tropospheric warming. More aspects of the vertical structure of tropospheric temperature change could be obtained by using combinations and differences of the MSU channels (e.g., Fu & Johanson, 2005), but we leave that as an exercise for future work.

4.2. Latitude and Seasonal Behavior

The latitude versus month variations in MSU2 tropospheric trends (Figures 3a and 3b) reveal patterns of significant warming throughout low to middle latitudes throughout the year, extending to northern middle and high latitudes during boreal summer (approximately April–October). A relative maximum in MSU2 tropospheric warming occurs in the NH extratropics (~30–70°N) during summer in both model and observations (Figure 4a). In this region there is low spread of temperature anomalies among model realizations (Figure 5a), demonstrating a strongly forced behavior, and observations closely follow the model. Tropospheric warming from MSU2 does not extend into high southern latitudes. The latitudinal fingerprint is similar in model and observations, although low-latitude warming extends farther southward in the WACCM ensemble (~50°S) compared to ~35°S in the observations (Figures 3a and 3b). This is one source of difference in the global mean MSU2 trends between observations and model results.

Temperature trends in the troposphere and stratosphere show relatively small spread among model realizations in low to middle latitudes but large variability in polar regions (Figure 2b), especially in the stratosphere during winter-spring seasons. This is one of the important results from the ensemble WACCM calculations, highlighting large internal variability in high-latitude trend results derived from a relatively short 36 year sample. In such a situation, observed trends should not be interpreted as a forced response. This behavior is analogous to the large variability in regional climate trends derived from ensemble climate model simulations, as shown in Deser et al. (2012). While the five members from WACCM are not a large ensemble, it is enough to highlight regions of enhanced variability.

Long-term changes in the MSU4 are small and negative over most of the globe; in low latitudes MSU4 reflects a weighted average of upper troposphere warming and LS cooling (Figure 2a). The observed MSU4 has slightly stronger cooling than MSU4 synthesized from the WACCM runs, similar to other CMIP5 or CCMval models (Thompson

Table 3

MSU2 and MSU3 Trends and 2 Sigma Uncertainties (as in Table 1) but Derived From a Simple Linear Regression Model Including Only Linear Fit (no Ancillary Proxy Terms) and Including the Volcanic Influenced Time Periods

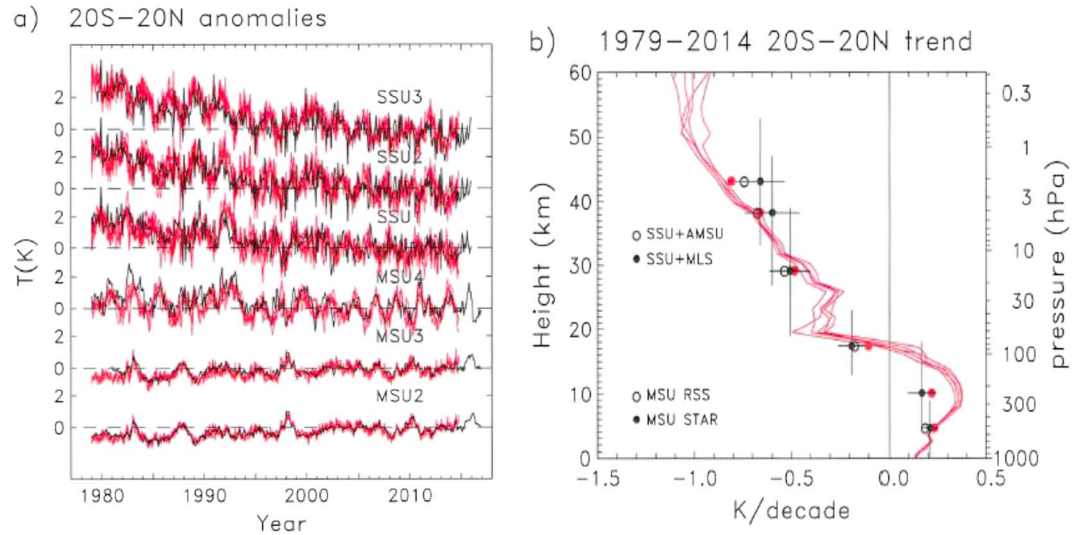| Data set	Global average	20°N-S
RSS MSU2	0.12 (0.05)	0.13 (0.07)
STAR MSU3	0.09 (0.06)	0.09 (0.09)
STAR MSU2	0.13 (0.05)	0.15 (0.08)
WACCM MSU3	0.07 (0.03)	0.15 (0.03)
WACCM MSU2	0.15 (0.02)	0.17 (0.03)

Figure A1. (a) Time series of 20°N-S average deseasonalized temperature anomalies for each of the MSU and SSU channels. Black lines shows observations (from STAR MSU and SSU + MLS data), and red lines show WACCM results. (b) Vertical profile of 20°N-S average temperature trends over 1979–2014 derived from satellite measurements and the WACCM realizations. Details are the same as in Figure 2a.

et al., 2012), although the differences are small. Much of this difference originates from slightly stronger observed low-latitude MSU4 cooling during approximately July–November, which is absent in the WACCM ensemble (Figures 3c and 3d). Strong MSU4 cooling is found in the Antarctic tied to development of the ozone hole, with the fingerprint of cooling extending from polar spring to midlatitudes during summer in both observations and model simulations (Figures 3c and 3d). Lower stratospheric polar spring cooling in the model extends downward enough to be sampled by MSU2 (Figure 3b), and evidence of this is seen in observed MSU2 trends (Figure 3a).

In the upper stratosphere, small annual average cooling occurs over Antarctica compared to low latitudes and also compared to the Arctic, that is, there is a hemispheric asymmetry in long-term upper stratosphere temperature changes. This behavior occurs in observations and four of the five model realizations (Figure 2b). This hemispheric asymmetry is not well understood. Small polar trends could reflect the influence of global upper stratosphere ozone losses during 1979–2014 most strongly impacting temperatures over low-latitude sunlit regions, although such trend gradients are not observed in the NH. This asymmetry may suggest an influence of long-term stratospheric circulation changes, stronger in the SH than in the NH. In both the model and observations the strongest latitudinal temperature trend gradients occur during SH winter, and the
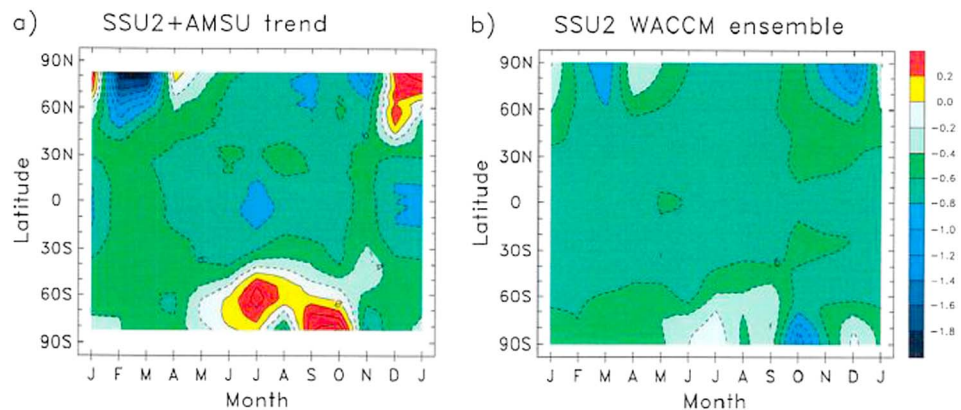

Figure A2. Latitude versus month temperature trends (K/decade) over 1979–2014 for SSU2, derived from (a) SSU2 + AMSU observations and (b) WACCM ensemble. None of the trends in the winter polar regions in either hemisphere are statistically significant in the observations or the model simulation.
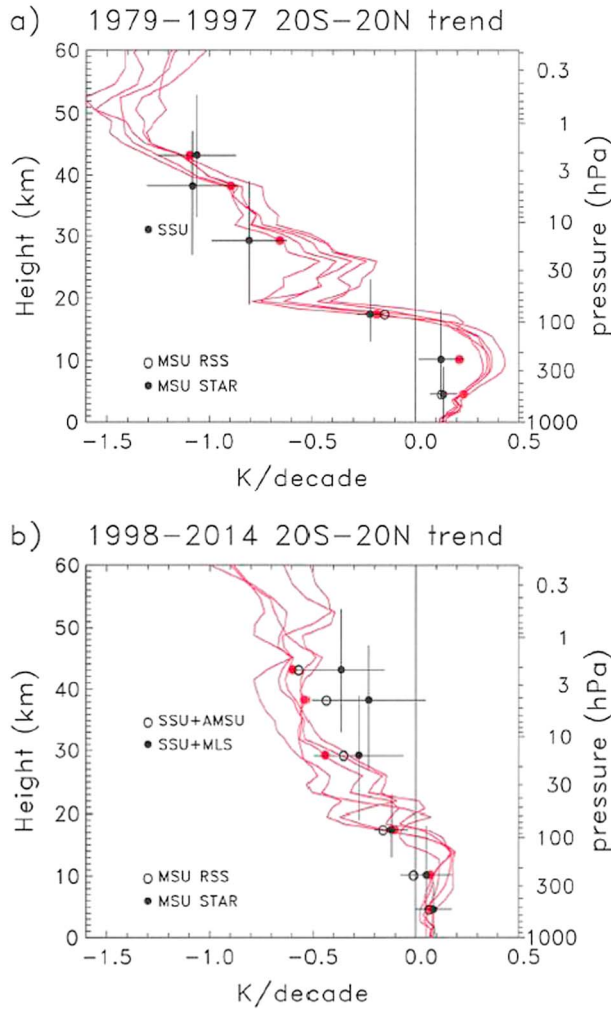
Figure A3. Vertical profiles of 20°N-S average temperature trends for (a) 1979–1997 and (b) 1998–2014, comparing satellite observations to WACCM results. Details are the same as in Figure 2a.

model shows a balanced thermal wind response of weakened polar night jet and shifting of large-scale wave drag to higher latitudes. This shifting wave drag is confined to the stratosphere, with little influence of changing wave fluxes from the troposphere in the model.

4.3. Temperature Response to Evolving Stratospheric Ozone

The stratospheric thermal response to evolving ozone is strong and shows agreement between model and observations. Stratospheric ozone in the model decreases until the late 1990s and increases thereafter in response to specified changes in ODS, and the model shows approximate agreement with ozone observations in the global upper stratosphere (Figure 6a) and in the Antarctic spring lower stratosphere (Figure 6b). Temperature trends in the upper stratosphere for the ozone decline period (1979–1997) show 2–3 times stronger cooling compared to the partial recovery period (1998–2014).

The Antarctic lower stratosphere shows the well-known cooling in response to development of the ozone hole over 1979–1997, followed by warming after 1998, as shown for the annual average model trends in Figure 7. Antarctic lower stratosphere MSU4 changes occur primarily during October–December (Figure 10), and while there is substantial variability among the model realizations, the approximate match to monthly trends derived from MSU4 observations is striking. The observed Antarctic warming in MSU4 after 1998 is a novel result; trends for the individual months October–December are marginally significant, but averages over October–November are more significant, although trends and significance levels differ between RSS and STAR data. Regardless of precise significance levels, the characteristic spatial and temporal behavior of the observed trends, and congruence with the WACCM simulations, provides convincing evidence that healing of the ozone hole reported in Solomon et al. (2016) is being reflected in observed temperature trends for the Antarctic lower stratosphere. A similar conclusion regarding Antarctic temperature trends has been reported by Solomon et al. (2017), based on (Modern-Era Retrospective Analysis for Research and Applications-2) MERRA2 reanalysis data. Overall, the observed temperature responses to stratospheric ozone changes, in both the lower and upper stratosphere, provide further evidence for anthropogenic influence on stratospheric temperatures.
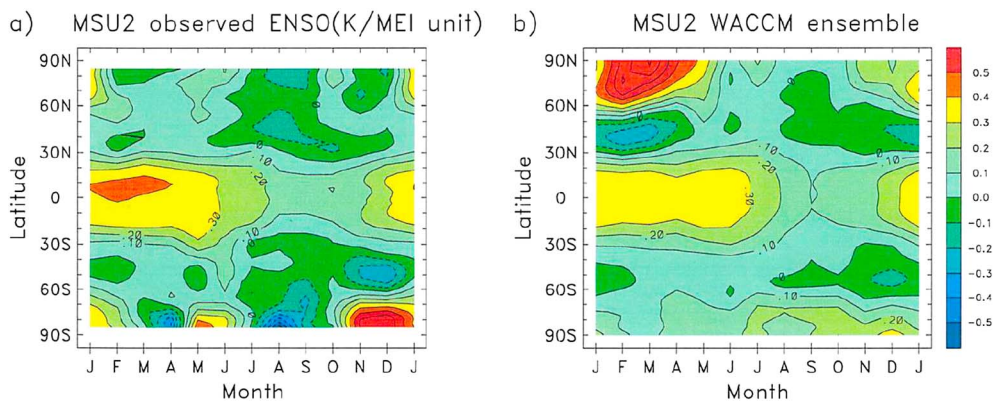

Figure A4. Latitude versus month plots of the ENSO regression of MSU2 tropospheric temperatures from (a) STAR observations and (b) WACCM ensemble. Units are K/(MEI index). The north-south see-saw patterns during boreal winter in the WACCM ensemble are evident in each of the model realizations but are absent in observations.

There is much stronger tropospheric warming for the period 1979–1997 compared to 1998–2014 (Figures 7 and 8), which reflects the stronger (imposed) SST trends for the first half of the record. The weaker trends for 1998–2014 are related to the so-called tropospheric warming "hiatus," and closely linked to SST behavior (Kosaka & Xie, 2013). It is natural to ask if this forced tropospheric behavior has an influence on stratospheric temperatures, possibly aliasing onto changes we have ascribed to GHG and ODS. The answer is probably "no," because previous calculations (Polvani & Solomon, 2012; Oberländer et al., 2013) have isolated the separate effects of SSTs, GHG, and ODS on troposphere-stratosphere temperature changes and clearly shown that SSTs strongly influence the troposphere and very lowest stratosphere but have little influence above ~20 km. Hence, we are confident in attributing the observed and modeled stratospheric temperature changes to the combined effects of GHG and ODS, with little influence from the SST-linked tropospheric warming hiatus.

Appendix A: Additional Observations Versus Model Comparisons

We include here a few additional diagnostics comparing observations versus model temperature variability. Figure A1 shows time series and vertical profile temperature trends over 1979–2014 for the deep tropics (20°N-S). Trends in the deep tropics are interesting because the tropospheric vertical profile is expected to reflect amplification of surface warming (e.g., Santer et al., 2005), as clearly seen for the WACCM results in Figure A1b. Latitude versus month temperature trends for the upper stratosphere (SSU2) are included in Figure A2, showing observed versus model agreement outside of winter polar regions (where internal variability is large). Deep tropical (20°N-S) temperature trends for the separate periods 1979–1997 and 1998–2014 are shown in Figure A3, highlighting large differences between these periods for both the troposphere and stratosphere. Figure A4 shows the ENSO regression signal in tropospheric temperatures (MSU2) as a function of month and latitude, highlighting a deep tropical temperature response maximizing in boreal winter for both observations and model simulation.

References

Aquila, V., Swartz, W. H., Waugh, D. W., Colarco, P. R., Pawson, S., Polvani, L. M., & Stolarski, R. S. (2016). Isolating the roles of different forcing agents in global stratospheric temperature changes using model integrations with incrementally added single forcings. *Journal of Geophysical Research: Atmospheres*, 121, 8067–8082. https://doi.org/10.1002/2015JD023841

Bourassa, A. E., Roth, C. Z., Zawada, D. J., Rieger, L. A., McLinden, C. A., & Degenstein, D. A. (2017). Drift corrected Odin-OSIRIS ozone product: Algorithm and updated stratospheric ozone trends. *Atmospheric Measurement Techniques Discussions*. https://doi.org/10.5194/amt-2017-229

Calvo, N., Garcia, R. R., & Kinnison, D. E. (2017). Revisiting Southern Hemisphere polar stratospheric temperature trends in WACCM: The role of dynamical forcing. *Geophysical Research Letters*, 44, 3402–3410. https://doi.org/10.1002/2017GL072792

Deser, C., Phillips, A. S., Bourdette, V., & Teng, H. (2012). Uncertainty in climate change projections: The role of internal variability. *Climate Dynamics*, 38, 527–546. https://doi.org/10.1007/s00382-010-0977-x

Efron, B., & Tibshirani, R. J. (1993). *An Introduction to the Bootstrap* (pp. 436). New York: Chapman and Hall.

Forster, P. M., Fomichev, V. I., Rozanov, E., Cagnazzo, C., Jonsson, A. I., Langematz, U., … Shibata, K. (2011). Evaluation of radiation scheme performance within chemistry climate models. *Journal of Geophysical Research*, 116, D10302. https://doi.org/10.1029/2010JD015361

Froidevaux, L., Anderson, J., Wang, H.-J., Fuller, R. A., Schwartz, M. J., Santee, M. L., … McCormick, M. P. (2015). Global ozone chemistry and related trace gas data records for the stratosphere (GOZCARDS): Methodology and sample results with a focus on HCl, H₂O, and O₃. *Atmospheric Chemistry and Physics*, 15, 10,471–10,507. https://doi.org/10.5194/acp-15-10471-2015

Free, M. (2011). The seasonal structure of temperature trends in the tropical lower stratosphere. *Journal of Climate*, 24, 859–866.

Fu, Q., & Johanson, C. M. (2005). Satellite-derived vertical dependence of tropical tropospheric temperature trends. *Geophysical Research Letters*, 32, L10703. https://doi.org/10.1029/2004GL022266

Fu, Q., Solomon, S., & Lin, P. (2010). On the seasonal dependence of tropical lower-stratosphere temperature trends. *Atmospheric Chemistry and Physics*, 10, 2643–2653.

Fu, Q., Lin, P., Solomon, S., & Hartmann, D. L. (2015). Observational evidence of strengthening of the Brewer-Dobson circulation since 1980. *Journal of Geophysical Research: Atmospheres*, 120, 10,214–10,228. https://doi.org/10.1002/2015JD023657

Garcia, R. R., & Randel, W. J. (2008). Acceleration of the Brewer-Dobson circulation due to increases in greenhouse gases. *Journal of the Atmospheric Sciences*, 65, 2731–2739.

Garcia, R. R., Marsh, D., Kinnison, D. E., Boville, B., & Sassi, F. (2007). Simulations of secular trends in the middle atmosphere, 1950–2003. *Journal of Geophysical Research*, 112, D09301. https://doi.org/10.1029/2006JD007485

Garcia, R. R., Smith, A. K., Kinnison, D. E., de la Cámara, Á., & Murphy, D. J. (2017). Modification of the gravity wave parameterization in the Whole Atmosphere Community Climate Model: Motivation and results. *Journal of the Atmospheric Sciences*, 74, 275–291. https://doi.org/10.1175/JAS-D-16-0104.1

Gillett, N., & Thompson, D. W. J. (2003). Simulation of recent Southern Hemisphere climate change. *Science*, 302, 273–275.

Gillett, N. P., Akiyoshi, H., Bekki, S., Braesicke, P., Eyring, V., Garcia, R., … Shibata, K. (2011). Attribution of observed changes in stratospheric ozone and temperature. *Atmospheric Chemistry and Physics*, 11, 599–609.

Hartmann, D. L., Klein Tank, A. M. G., Rusticucci, M., Alexander, L. V., Brönnimann, S., Charabi, Y., … Zhai, P. M. (2013). Observations: Atmosphere and surface. In T. F. Stocker, et al. (Eds.), *Climate Change 2013: The Physical Science Basis. Contribution of Working Group I to the Fifth Assessment Report of the Intergovernmental Panel on Climate Change* (pp. 159–254). Cambridge, UK, and New York: Cambridge University Press.

Hurrell, J. W., Hack, J. J., Shea, D., Caron, J. M., & Rosinski, J. (2008). A new sea surface temperature and sea ice boundary data set for the Community Atmosphere Model. *Journal of Climate*, *21*, 5145–5153. https://doi.org/10.1175/2008JCLI2292.1

Ivy, D. J., Solomon, S., & Rieder, H. E. (2016). Radiative and dynamical influences on polar stratospheric temperature trends. *Journal of Climate*, *29*, 4927–4938.

Kinnison, D. E., Brasseur, G. P., Walters, S., Garcia, R. R., Marsh, D. R., Sassi, F., … Simmons, A. J. (2007). Sensitivity of chemical tracers to meteorological parameters in the MOZART-3 chemical transport model. *Journal of Geophysical Research*, *112*, D20302. https://doi.org/10.1029/2006JD007879

Kosaka, Y., & Xie, S.-P. (2013). Recent global-warming hiatus tied to equatorial Pacific surface cooling. *Nature*, *501*, 403–407. https://doi.org/10.1038/nature12534

Kyrölä, E., Laine, M., Sofieva, V., Tamminen, J., Päivärinta, S.-M., Tukiainen, S., … Thomason, L. (2013). Combined SAGE II-GOMOS ozone profile data set 1984–2011 and trend analysis of the vertical distribution of ozone. *Atmospheric Chemistry and Physics*, *13*, 10,645–10,658.

Lin, S.-J. (2004). A"vertically-Lagrangian" finite-volume dynamical core for global atmospheric models. *Monthly Weather Review*, *132*, 2293–2307.

Lin, P., Fu, Q., Solomon, S., & Wallace, J. M. (2009). Temperature trend patterns in Southern Hemisphere high latitudes: Novel indicators of stratospheric changes. *Journal of Climate*, *22*, 6325–6341.

Marsh, D. R., Mills, M. J., Kinnison, D. E., Lamarque, J.-F., Calvo, N., & Polvani, L. M. (2013). Climate change from 1850 to 2005 simulated in CESM1(WACCM), 73727391. *Journal of Climate*, *26*(19). https://doi.org/10.1175/JCLI-D-12-00558.1

Manabe, S., & Wetherald, R. (1967). Thermal equilibrium of the atmosphere with a given distribution of relative humidity. *Journal of the Atmospheric Sciences*, *24*, 241–259.

Matthes, K., Marsh, D. R., Garcia, R. R., Kinnison, D. E., Sassi, F., & Walters, S. (2010). Role of the QBO in modulating the influence of the 11 year solar cycle on the atmosphere using constant forcings. *Journal of Geophysical Research*, *115*, D18110. https://doi.org/10.1029/2009JD013020

McLandress, C., Shepherd, T. G., Jonsson, A. I., von Clarmann, T., & Funke, B. (2015). A method for merging nadir-sounding climate records, with an application to the global-mean stratospheric temperature data sets from SSU and AMSU. *Atmospheric Chemistry and Physics*, *15*, 9271–9284. https://doi.org/10.5194/acp-15-9271-2015

Mears, C. A., & Wentz, F. J. (2009). Construction of the remote sensing systems V3.2 atmospheric temperature records from the MSU and AMSU microwave sounders. *Journal of Atmospheric and Oceanic Technology*, *26*, 1040–1056.

Mears, C. A., & Wentz, F. J. (2016). Sensitivity of satellite-derived tropospheric temperature trends to the diurnal cycle adjustment. *Journal of Climate*, *29*, 3629–3646.

Mitchell, D. M. (2016). Attributing the forced components of observed stratospheric temperature variability to external drivers. *Quarterly Journal of the Royal Meteorological Society*, *142*, 1041–1047. https://doi.org/10.1002/qj.2707

Morgenstern, O., Hegglin, M. I., Rozanov, E., O'Connor, F. M., Abraham, N. L., Akiyoshi, H., … Zeng, G. (2017). Review of the global models used within the Chemistry-Climate Model Initiative (CCMI). *Geoscientific Model Development*. https://doi.org/10.5194/gmd-10-639-2017

Neale, R. B., Richter, J., Park, S., Lauritzen, P. H., Vavrus, S. J., Rasch, P. J., & Zhang, M. (2013). The mean climate of the Community Atmosphere Model (CAM4) in forced SST and fully coupled experiments. *Journal of Climate*, *26*(14), 5150–5168. https://doi.org/10.1175/JCLI-D-12-00236.1

Oberländer, S., Langematz, U., & Meul, S. (2013). Unraveling impact factors for future changes in the Brewer-Dobson circulation. *Journal of Geophysical Research: Atmospheres*, *118*, 10,296–10,312. https://doi.org/10.1002/jgrd.50775

Polvani, L. M., & Solomon, S. (2012). The signature of ozone depletion on tropical temperature trends, as revealed by their seasonal cycle in model integrations with single forcings. *Journal of Geophysical Research*, *117*, D17102. https://doi.org/10.1029/2012JD017719

Polvani, L. M., Wang, L., Aquila, V., & Waugh, D. W. (2017). The impact of ozone depleting substances on tropical upwelling, as revealed by the absence of lower stratosphere cooling since the late 1990s. *Journal of Climate*, *30*, 2523–2534. https://doi.org/10.1175/JCLI-D-16-0532.1

Ramaswamy, V. and M. D. Schwarzkopf, 2002: Effects of ozone and well-mixed gases on annual-mean stratospheric temperature trends, *Geophysical Research Letters, 29*(22), 2064. https://doi.org/10.1029/2002GL015141

Randel, W., & Wu, F. (1999). Cooling of the Arctic and Antarctic polar stratospheres due to ozone depletion. *Journal of Climate*, *12*, 1467–1479.

Randel, W. J., Smith, A. K., Wu, F., Zou, C.-Z., & Qian, H. (2016). Stratospheric temperature trends over 1979–2015 derived from combined SSU, MLS and SABER satellite observations. *Journal of Climate*, *29*, 4843–4859. https://doi.org/10.1175/JCLI-D-15-0629.1

Santer, B. D., Wigley, T. M. L., Doutriaux, C., Boyle, J. S., Hansen, J. E., Jones, P. D., … Taylor, K. E. (2001). Accounting for the effects of volcanoes and ENSO in comparisons of modeled and observed temperature trends. *Journal of Geophysical Research*, *106*, 28,033–28,059. https://doi.org/10.1029/2000JD000189

Santer, B. D., Wigley, T. M., Mears, C., Wentz, F. J., Klein, S. A., Seidel, D. J., … Schmidt, G. A. (2005). Amplification of surface temperature trends and variability in the tropical atmosphere. *Science*, *309*(5,740), 1551–1556.

Santer, B. D., Thorne, P. W., Haimberger, L., Taylor, K. E., Wigley, T. M. L., Lanzante, J. R., … Wentz, F. J. (2008). Consistency of modelled and observed temperature trends in the tropical troposphere. *International Journal of Climatology*, *28*, 1703–1722. https://doi.org/10.1002/joc.1756

Santer, B. D., Painter, J. F., Bonfils, C., Mears, C. A., Solomon, S., Wigley, T. M. L., … Wentz, F. J. (2013). Human and natural influences on the changing thermal structure of the atmosphere. *Proceedings of the National Academy of Sciences of the United States of America*, *110*, 17,235–17,240. https://doi.org/10.1073/pnas.1305332110

Santer, B. D., Solomon, S., Pallotta, G., Mears, C., Po-Chedley, S., Fu, Q., … Bonfils, C. (2017). Comparing tropospheric warming in climate models and satellite data. *Journal of Climate*, *30*, 373–392.

Screen, J. A., & Simmonds, I. (2010). The central role of diminishing sea-ice in recent Arctic temperature amplification. *Nature*, *464*, 1334–1337.

Seidel, D. J., Gillett, N. P., Lanzante, J. R., Shine, K. P., & Thorne, P. W. (2011). Stratospheric temperature trends: Our evolving understanding. *Wiley Interdisciplinary Reviews: Climate Change*, *2*, 592–616.

Seidel, D. J., Li, J., Mears, C., Moradi, I., Nash, J., Randel, W. J., … Zou, C.-Z. (2016). Stratospheric temperature changes during the satellite era. *Journal of Geophysical Research: Atmospheres*, *121*, 664–681. https://doi.org/10.1002/2015JD024039

Shine, K. P., Bourqui, M. S., PMdeF, F., Hare, S. H. E., Langematz, U., Braesicke, P., … Schwarzkopf, M. D. (2003). A comparison of model-predicted trends in stratospheric temperatures. *Quarterly Journal of the Royal Meteorological Society*, *129*, 1565–1588. https://doi.org/10.1256/qj.02.186

Solomon, S., Kinnison, D. E., Bandoro, J., & Garcia, R. (2015). Simulations of polar ozone depletion: An update. *Journal of Geophysical Research: Atmospheres*, *120*, 7958–7974. https://doi.org/10.1002/2015JD0233652015

Solomon, S., Ivy, D. J., Kinnison, D., Mills, M. J., Neely, R. R. III, & Schmidt, A. (2016). Emergence of healing in the Antarctic ozone hole. *Science*. https://doi.org/10.1126/science.aae0061

Solomon, S., Ivy, D., Gupta, M., Bandoro, J., Santer, B., Fu, Q., … Mills, M. (2017). Mirrored changes in Antarctic ozone and temperature in the 20th versus 21st centuries. *Journal of Geophysical Research: Atmospheres*, *122*, 8940–8950. https://doi.org/10.1002/2017JD026719

Stratospheric Processes and their Role in Climate (2010). SPARC Report on the Evaluation of Chemistry-Climate Models. In V. Eyring, T. G. Shepherd, & D. W. Waugh (Eds.) (SPARC Report No. 5, WCRP-132, WMO/TD-No.1526). http://www.sparc-climate.org

Stevenson, D. S., Young, P. J., Naik, V., Lamarque, J.-F., Shindell, D. T., Voulgarakis, A., … Archibald, A. (2013). Tropospheric ozone changes, radiative forcing and attribution to emissions in the Atmospheric Chemistry and Climate Model Intercomparison Project (ACCMIP). *Atmospheric Chemistry and Physics*, *13*, 3063–3085. https://doi.org/10.5194/acp-13-3063-2013

Stolarski, R. S., Douglass, A. R., Newman, P. A., Pawson, S., & Schoeberl, M. R. (2010). Relative contribution of greenhouse gases and ozone-depleting substances to temperature trends in the stratosphere: A chemistry-climate model study. *Journal of Climate*, *23*, 28–42. https://doi.org/10.1175/2009JCLI2955.1

Taylor, K. E., Stouffer, R. J., & Meehl, G. A. (2012). An overview of CMIP5 and the experiment design. *Bulletin of the American Meteorological Society*, *93*, 485–498.

Thompson, D. W. J., & Solomon, S. (2002). Interpretation of recent Southern Hemisphere climate change. *Science*, *296*, 895–899.

Thompson, D. W. J., Seidel, D. J., Randel, W. J., Zou, C.-Z., Butler, A. H., Lin, R., … Osso, A. (2012). The mystery of recent stratospheric temperature trends. *Nature*, *491*, 692–697. https://doi.org/10.1038/nature11579

Wallace, J. M., Panetta, L., & Estberg, J. (1993). A phase-space representation of the equatorial stratospheric quasi-biennial oscillation. *Journal of the Atmospheric Sciences*, *50*, 1751–1762.

Wegner, T., Kinnison, D. E., Garcia, R. R., Madronich, S., & Solomon, S. (2013). Polar stratospheric clouds in SD-WACCM4. *Journal of Geophysical Research: Atmospheres*, *118*, 4991–5002. https://doi.org/10.1002/jgrd.50415

Wolter, K., & Timlin, M. S. (2011). El Niño/Southern Oscillation behaviour since 1871 as diagnosed in an extended multivariate ENSO index (MEI.ext). *International Journal of Climatology*, *31*, 1074–1087. https://doi.org/10.1002/joc.2336

Young, P. J., Butler, A. H., Calvo, N., Haimberger, L., Kushner, P. J., Marsh, D. R., … Rosenlof, K. H. (2013). Agreement in late twentieth century Southern Hemisphere stratospheric temperature trends in observations and CCMVal-2, CMIP3 and CMIP5 models. *Journal of Geophysical Research: Atmospheres*, *118*, 605–613. https://doi.org/10.1002/jgrd.50126

Zhao, L., Xu, J., Powell, A. M., Jiang, Z., & Wang, D. (2016). Use of SSU/MSU satellite observations to validate upper atmospheric temperature trends in CMIP5 simulations. *Remote Sensing*, *8*, 13. https://doi.org/10.3390/rs8010013

Zou, C.-Z., Goldberg, M., Cheng, Z., Grody, N., Sullivan, J., Cao, C., & Tarpley, D. (2006). Recalibration of Microwave Sounding Unit for climate studies using simultaneous nadir overpasses. *Journal of Geophysical Research*, *111*, D19114. https://doi.org/10.1029/2005JD006798

Zou, C.-Z., & Wang, W. (2011). Inter-satellite calibration of AMSU-A observations for weather and climate applications. *Journal of Geophysical Research: Atmospheres*, *116*, D23113. https://doi.org/10.1029/2011JD016205

Zou, C.-Z., Qian, H., Wang, W., Wang, L., & Long, C. (2014). Recalibration and merging of SSU observations for stratospheric temperature trend studies. *Journal of Geophysical Research: Atmospheres*, *119*, 13,180–13,205. https://doi.org/10.1002/2014JD021603

Zou, C.-Z., & Qian, H. (2016). Stratospheric temperature climate data record from merged SSU and AMSU-A observations. *Journal of Atmospheric and Oceanic Technology*, *33*, 1967–1984. https://doi.org/10.1175/JTECH-D-16-0018.1